Macromolecules

ARTICLE

pubs.acs.org/Macromolecules

Influence of the Supramolecular Organization on the Magnetic Properties of Poly(3-alkylthiophene)s in Their Neutral State

Steven Vandeleene,[†,⊥] Mihaela Jivanescu,[‡,⊥] André Stesmans,[‡,⊥] Jo Cuppens,[§,⊥] Margriet J. Van Bael,[§,⊥] Thierry Verbiest,[†,⊥] and Guy Koeckelberghs*[,†,⊥]

[†]Laboratory of Molecular Electronics and Photonics, Katholieke Universiteit Leuven, Celestijnenlaan 200F, B-3001 Heverlee, Belgium

[‡]Semiconductor Physics Laboratory, Katholieke Universiteit Leuven, Celestijnenlaan 200D, B-3001 Leuven, Belgium

[§]Laboratory of Solid State Physics and Magnetism, Katholieke Universiteit Leuven, Celestijnenlaan 200D, B-3001 Leuven, Belgium

[⊥]Institute for Nanoscale Physics and Chemistry (INPAC), University of Leuven, B-3001 Leuven, Belgium

Supporting Information

ABSTRACT: The influence of the supramolecular behavior on the magnetic properties of head-to-tail coupled poly(3-alkylthiophene)s (P3AT) is reported. Samples with a different molar mass were prepared, and differences in their behavior were illustrated by UV−vis and CD spectroscopy. In addition, tuning of the supramolecular organization was also accomplished by applying thermal annealing. ESR spectroscopy was performed on powder samples. From the line features, information on the nature of the unpaired spins, the mobility, and the supramolecular order of the sample was derived. These spins are paramagnetic. SQUID magnetometry, in contrast, shows for all samples a ferromagnetic behavior at 5 K and superparamagnetism at 300 K. The coercivity does not depend on the degree of supramolecular order but is inherent to the molecular structure and, related to this, the π-interactions. The saturation magnetization, on the contrary, seems to be mainly influenced by the fraction of planarized polymer chains.

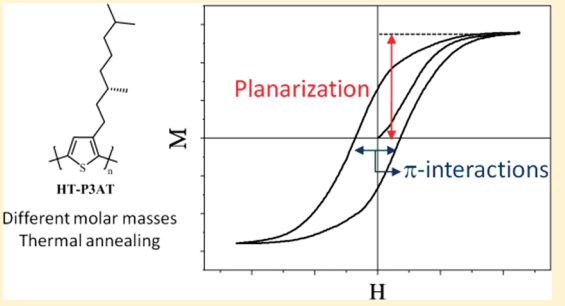

INTRODUCTION

For almost three decades, π-conjugated polymers have been explored extensively. Besides their optical, electrical, and electronic properties,[1] also the magnetic behavior has been investigated, albeit to a lesser extent. In order for an organic compound to exhibit ferromagnetism, unpaired electrons (spins) should be present. Mostly, spins are intrinsic[2−4] to the material or introduced as radicals, carbenes, or by oxidation.[2,3,5] A second requirement is a pathway by which unpaired spins can mutually interact (spin coupling).[6] In this point of view, a conjugated π-system is ideal to act as a (ferro)magnetic linker between different spins. However, the substitution pattern and the connectivity are crucial parameters to have ferromagnetic spin coupling, aligning spins in the same direction of an external magnetic field.[7] Quite some "high-spin" molecules,[8,9] oligomers,[10] and polymers[11−14] have been reported based on this approach, and remarkable advances have been achieved.

Besides the "high-spin" molecules, also some typical conjugated polymers were reported, showing magnetic behavior under very specific conditions. Typical examples are poly(aniline)s,[15−18] poly(pyrrole),[19] regioirregular poly(3-alkylthiophene)s,[20−24] and (substituted) poly(acetylene)s.[25] In all these examples, the materials were chemically or electrochemically doped, introducing spins (polarons). In contrast to these results, we have previously reported on the magnetic behavior of neutral (undoped) poly(thiophene)s carrying an alkyl, alkoxy, or alkylthio side chain.[26]

A comparison of the ESR and SQUID data reveals the presence of (at least) two spin systems. A first electron spin system gives rise to a paramagnetic behavior. A second spin system (of which the origin is unknown) results in a superparamagnetic behavior at 300 K and (for most polymers) a ferromagnetic behavior at 5 K. The ESR-active system is not responsible for the ferromagnetic behavior at 5 K. This has been concluded from the fact that it exhibits a paramagnetic behavior and that there is a large discrepancy between the number of spins ($S = 1/2$), determined by ESR, and the number of Bohr magnetons (magnetic moment of an electron) measured by SQUID magnetometry. Concerning the presence of ferromagnetism and the coercivity, it was found that polymers in which strong π-interactions between stacked polymer chains are present show the highest coercivity. Therefore, it can be hypothesized that these π-interactions determine the ferromagnetic behavior (coercivity).

In this article, the influence of supramolecular organization and π-stacking of a chiral substituted, head-to-tail coupled poly(3-alkylthiophene) (HT-P3AT) on its magnetic behavior is investigated (Figure 1). First, since aggregate formation is influenced by the molar mass of these polymers, samples with different molar masses were prepared by fractionation. Differences in their

Received: May 6, 2011
Revised: May 23, 2011
Published: June 02, 2011

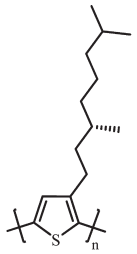

HT-P3AT

$\overline{M}_n$ = 7.0 kg/mol **P1** $\overline{M}_n$ = 12.5 kg/mol **P3**
$\overline{M}_n$ = 10.3 kg/mol **P2** $\overline{M}_n$ = 16.0 kg/mol **P4**

Figure 1. Structure of the chiral HT-P3ATs **P1**−**4**.

supramolecular behavior are probed by UV−vis and circular dichroism (CD) spectroscopy, while the magnetic properties are evaluated by ESR spectroscopy and SQUID magnetometry. A chiral rather than an achiral substituent was preferred, since this allows the use of powerful chiroptical techniques which can provide important information on the supramolecular structure of the material. Second, supramolecular organization and resulting changes in the π-interactions were manipulated by thermal annealing[27] and the magnetic response was again investigated.

MATERIALS AND METHODS

Gel permeation chromatography (GPC) measurements were done with a Shimadzu 10A apparatus with a tunable absorbance detector and a differential refractometer in tetrahydrofuran (THF) as eluent toward polystyrene standards.

UV−vis and CD spectra were recorded with a Varian Cary 400 and a JASCO 62 DS apparatus, respectively. The DSC experiments were performed on a DSC 7 from Perkin-Elmer

Films were prepared by spin-coating from chloroform solutions on a glass substrate. To vary the film thickness, polymer solutions with different concentrations (9.4, 24, and 40 mg/mL) were used and the preparation parameters were kept constant (spinning speed: 1500 rpm; spinning time: 30 s). A Mettler-Toledo FP900 Thermosystem was used for sample annealing. Polymer films were heated at 170 °C for several minutes. Afterward, fast cooling was obtained by dipping the film in methanol, cooled at −78 °C, and dried under an air flow. Slow cooling was accomplished at a cooling rate of −10 °C/min. Powder samples, washed with an alcoholic hydrazine solution and methanol, were annealed (after drying) between two Teflon layers at 170 °C for several minutes. Fast cooling was obtained by dipping the Teflon layer in methanol, cooled at −78 °C, and dried under an air flow. Slow cooling of the powder samples was accomplished at a cooling rate of −10 °C/min. After thermal treatment, the powder samples were gently removed from the Teflon substrate.

The powders were weighted and stored under inert (argon) atmosphere. It should be stressed that Soxhlet extraction in essence delivers nickel-free polymer samples as previously motivated.[26]

Conventional continuous slow-passage X-band (~9.2 GHz) ESR measurements were carried out at room temperature using a Jeol FA100 spectrometer, where low microwave power ($P_\mu \leq 1$ mW) first-derivative absorption dP_μ/dB spectra were recorded through applying sinusoidal modulation (~100 kHz; amplitude $B_m \sim 0.35$ G) of the externally applied magnetic field B. Some observations were made in a mode-built K-band (~20.6 GHz) setup, as described elsewhere.[28] A comounted calibrated MgO:Mn^{2+} reference sample was used for absolute g factor and spin density (spin $S = 1/2$) calibration, with the latter performed through double numerical integration of the detected dP_μ/dB spectra. At X-band, the g values of the third and fourth lines of the Mn^{2+} (^{55}Mn; 100% natural abundance; nuclear spin $I = 5/2$) sextet were calibrated as 2.0338 ± 0.0001 and 1.9807 ± 0.0001, respectively. The attained absolute and relative accuracy is estimated at ~20% and ~5%, respectively. Signal averaging (typically ~50 scans) was routinely applied to enhance spectral quality.

SQUID-based magnetometry is carried out in a MPMS-XL magnetometer (Quantum Design). The powders are weighted, and a typical amount of 15 mg is fixed between small pieces of pure cotton wool inside the nonmagnetic plastic transparent sample tube. No capsules are used to hold the powder in order to avoid any magnetic contributions from the capsules interfering with the measured signal. The magnetic signal from the plastic sample tube with cotton wool (without the powder sample) is measured separately and shows a small diamagnetic contribution which is linear in applied field and can therefore be distinguished from nonlinear contributions from the powders. Magnetization was measured at different fixed temperatures as a function of magnetic field in RSO (reciprocating sample option) operation mode.

When measuring weak magnetic responses, one needs to be very cautious for (magnetic) contaminations, Therefore, working conditions were kept as clean as possible, and any contact of the sample powders with metals (spatula, etc.) was avoided. Moreover, control ESR experiments were performed on several samples before and after the SQUID measurements. No traces of ferromagnetic metal (Fe, Ni, etc.) contaminations could be detected in the ESR spectra.

Table 1. Molar Mass and DSC Data of P1−4

polymer	$\overline{M}_n$[a] (kg/mol)	D[b]	$\overline{X}_n$[c]	$\overline{X}_n$[d]	T_m[e] (°C)	ΔH_m[e] (J/g)
P1	7.0	1.2	32	17	103	8.7
P2	10.3	1.3	46	20	121	11.4
P3	12.5	1.2	56	28	131	16.1
P4	16.0	1.1	72	34	137	16.5

[a] Number-averaged molar mass. [b] Polydispersity, determined by GPC in THF, toward polystyrene standards. [c] Degree of polymerization, determined by GPC in THF, toward polystyrene standards. [d] Degree of polymerization, determined by relative integration of the inner and terminal methylene ^{1}H NMR resonances. [e] Measured by DSC with a heating rate of 20 °C/min; the second heating run was used.

RESULTS AND DISCUSSION

Materials. Regioregular, head-to-tail poly(3-alkylthiophene), substituted with a chiral alkyl side chain, was prepared by the Grignard metathesis procedure, described by McCullough and co-workers.[29] After polymerization, the crude polymer, having a polydispersity of 2.25, was precipitated in methanol, isolated, and fractionated.

The fractionation[30−33] of the crude polymer was accomplished by means of a Soxhlet extraction with different solvents. First, methanol and acetone were used to remove catalyst traces, unreacted monomers, and oligomers. Second, the polymer was extracted with *n*-pentane (**P1**), *n*-hexane (**P2**), dichloromethane (**P3**), and chloroform (**P4**). Finally, all isolated polymer fractions were concentrated, precipitated in ice-cooled methanol, filtrated, and dried in vacuo until a constant mass was reached. The number-averaged molar mass ($\overline{M}_n$) and polydispersity (D) of the isolated fractions were determined by GPC (GPC traces, see Figure S1) and are summarized in Table 1. The samples show a significant difference in molar mass, and in all cases, the polydispersity is below 1.3. The degree of polymerization was also calculated by relative integration of the inner and terminal methylene ^{1}H NMR resonances.

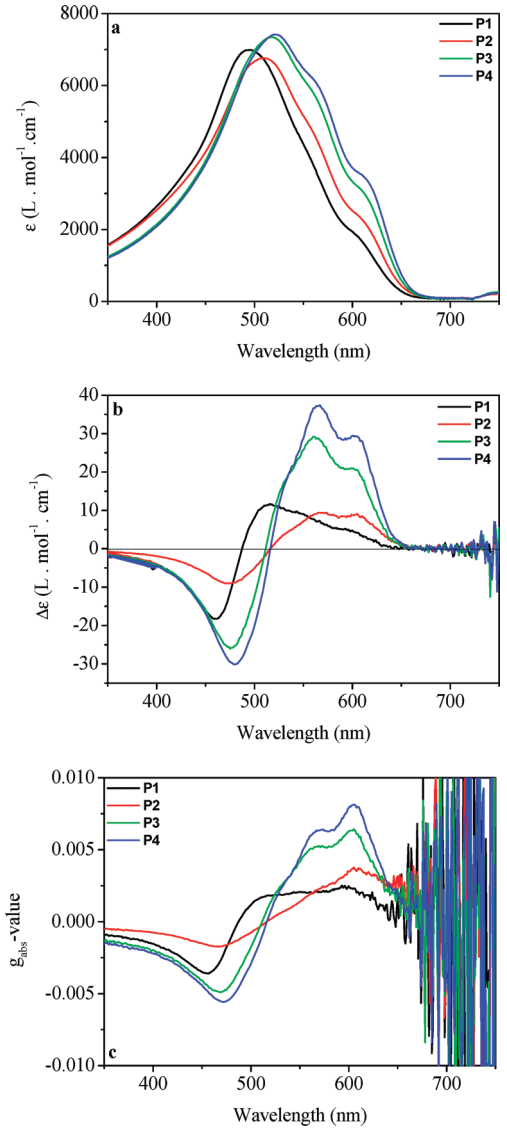

Figure 2. UV−vis spectra (a), CD spectra (b), and g_{abs} value (c) of **P1**−**4** in a mixture of chloroform and methanol (2/8).

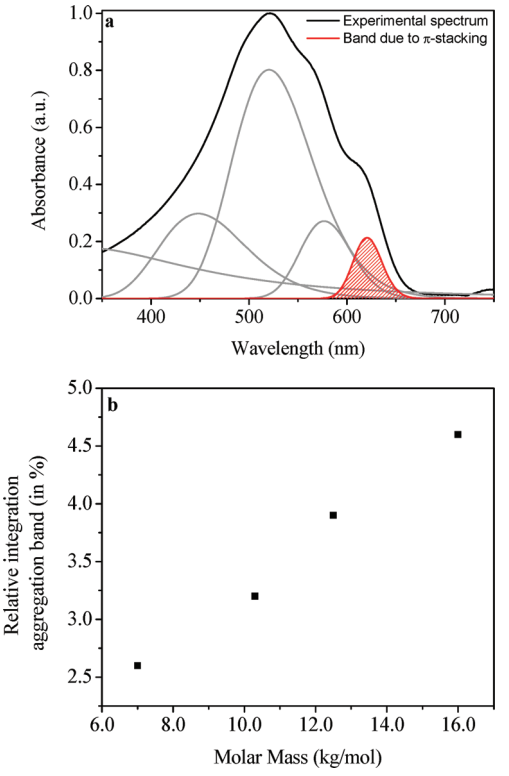

Figure 3. (a) Deconvolution of the UV−vis spectra, resolving the aggregation-related absorption band, shown for **P4**. (b) Relative integration of the aggregation-related absorption band (shaded peak) as a function of the molar mass, determined by GPC.

Chiroptical Behavior: Molar Mass Dependency. The supramolecular organization and π-stacking were investigated by UV−vis and CD spectroscopy. As ESR and SQUID measurements are typically performed on polymer powders, prepared by precipitation from methanol, a good approach to characterize differences between the polymer powders is by comparing the chiroptical behavior of **P1**−**4** in their aggregated form in solution.

The chiroptical behavior of **P1**−**4** was investigated both in good solvent and upon addition of nonsolvent. In good solvents, such as chloroform, the λ_{max} of **P1**−**4** is more or less equal (see Figure S3), indicating that the conjugation length of the actual "chromophore" is not limited by the degree of polymerization. However, when the solvent quality diminishes upon addition of methanol, aggregation is induced. In all cases, the UV−vis spectra (Figure 2a) show a red-shift of the λ_{max}, which is more pronounced for higher molar masses. In fact, the samples are composed of three "chromophores". One band (∼450 nm) arises from disordered, coiled polymer chains. A second transition (∼530 nm, with vibronic fine structure) is localized on planar, stacked chains. Finally, all samples show a red-shifted shoulder at around 615 nm. This distinct, low-energy absorption band can be attributed to a transition dipole moment, delocalized over multiple, aggregated polymer chains.[34,35] This phenomenon is, however, not limited to HT-P3AT.[36] Quite some semicrystalline, π-conjugated polymers show this very specific absorption band as well.[37,38] The occurrence of this aggregation-related absorption band is also visible in the CD spectrum (Figure 2b). While the first UV−vis transition is CD silent, the others give rise to Cotton effects. A bisignate Cotton effect, due to chiral exciton coupling, is associated with the planarized polymer chains. Also, a monosignate Cotton effect, corresponding to the red-shifted transition, is present, caused by a helically oriented transition dipole moment, delocalized over multiple polymer chains. The four polymer samples essentially differ in the relative ratio of the aggregation-related absorption band. This can already be observed by the more pronounced shoulder at 615 nm for **P4**, compared to **P1**. Also, the g_{abs} value ($= \Delta\varepsilon/\varepsilon$), which is a measure for the chirality of a system, was calculated (Figure 2c) and shows a maximum value of 7.5×10^{-3} for **P4**. Therefore, already as first evidence, UV−vis and CD spectra confirm that a higher crystalline fraction, in which the polymer strands are chirally stacked and mutually interact, is present in high molar mass polymers.

In order to quantify the aggregation-related absorption band, the different UV−vis spectra were deconvoluted as shown for **P4** in Figure 3 (see also Figure S4) using a linear programming method.[39] Figure 3b shows the relative, integrated absorption of the red-shift band as a function of the molar mass of the polymer samples. It is clear that a more intense aggregation-related absorption band correlates with higher molar masses. This observation

dx.doi.org/10.1021/ma201039x |*Macromolecules* 2011, 44, 4911–4919

complies with the observations made by other groups, using X-ray diffraction (XRD) and differential scanning calorimetry (DSC) on polymer samples having different molar masses.[40−42] High molar mass HT-P3AT has a higher crystalline fraction compared to low molecular mass HT-P3AT,[40,43] which is again confirmed by our results. As a consequence, the red-shifted absorption, for which π-interactions play a crucial role, is more pronounced in HT-P3ATs with high molar masses, as they show a higher degree of order.

In order to verify that the higher molar mass samples indeed have a higher degree of crystallinity, we performed some DSC experiments. All polymers are semicrystalline and show similar thermograms, suggesting that the same type of crystals is formed. This is in line with the fact that the molar mass does not change dramatically and remains in the region where chain-extended crystals are expected.[44,45] The melting temperature T_m and melting enthalpy (ΔH_m) were typically measured at the second heating run and are shown in Table 1. A similar behavior as found for poly(3-hexylthiophene) is present: both T_m and ΔH_m increase with $\overline{M}_n$. Since ΔH_m increases with increasing degree of crystallinity, it can be concluded that the degree of crystallinity indeed increases with increasing $\overline{M}_n$.

Chiroptical Behavior: Influence of Annealing. Not only the molar mass influences the aggregate formation. Also, thermal treatment of the polymer samples (annealing) has a significant influence on the amount, the shape, and the size of aggregates. To study the effect of annealing on the magnetic properties of HT-P3AT, several powder samples of **P3** were subjected to different heat treatments. The powders were gently pressed (1 ton/cm^2) to ensure a good thermal contact. Pressure has shown to influence the supramolecular structure of P3ATs as well.[46] However, the pressure required is several orders of magnitude higher. Here, we "press" the powder to ensure good thermal contact for the thermal annealing. In order to monitor the changes on a supramolecular level, films of **P3** were subjected to the same thermal treatment as the powders and were characterized by UV−vis and CD spectroscopy.

A film of **P3** was spin-coated (1500 rpm) from a chloroform solution (24.0 mg/mL), and the UV−vis and CD spectra were recorded (Figure 4), prior to any thermal treatment. A λ_{max} value of 520 nm is observed, which is quite common for aggregated HT-P3ATs. There is also a slight indication of the presence of the typical, aggregation-related absorption band around 615 nm. The CD spectrum (Figure 4b) clearly consists of a bisignate Cotton effect due to chiral exciton coupling. In addition, the monosignate Cotton effect, associated with the red-shifted band around 615 nm, is weakly present. Next, the polymer film was heated at 150 °C, well above T_m, for several minutes and immediately cooled down in methanol at −78 °C (**P3-fast**). After drying the sample under an air flow, the UV−vis and CD spectra were measured. Both spectra of the fast-cooled sample are almost identical to those of the spin-coated sample, prior to any annealing. If, however, the sample is heated at 150 °C for several minutes and subsequently slowly cooled down (cooling rate: −10 °C/min) (**P3-slow**), significant changes are observed in both the UV−vis and CD spectrum. The maximum absorption does not change significantly, but the spectrum shows a more defined fine structure. At 615 nm, the red-shifted, aggregation-related absorption band becomes more pronounced. Also in the CD spectrum, a monosignate Cotton effect, associated with the aggregation-related absorption band, is more intense. These observations suggest that the fraction of polymer segments,

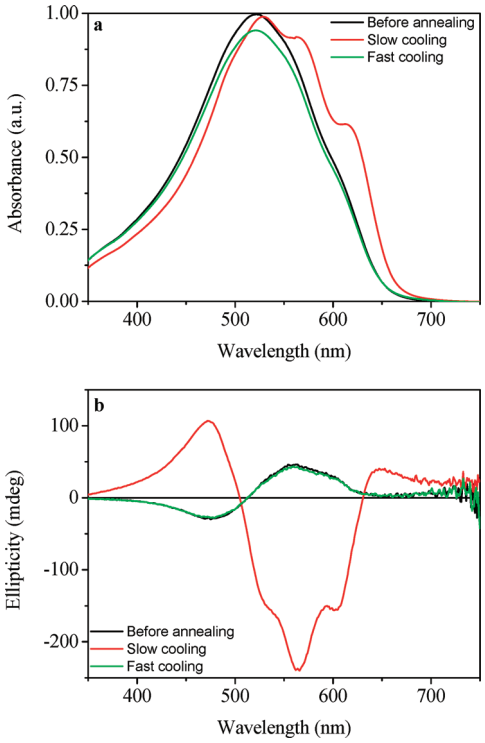

Figure 4. UV−vis (a) and CD spectra (b) of a **P3** film (spin-coated from a chloroform solution; 24.0 mg/mL; 1500 rpm) subjected to different annealing procedures.

interacting via π-interactions, is significantly higher. Besides the appearance of the monosignate Cotton effect in the CD spectrum, other remarkable changes are observed: the intensity of the CD signal has increased significantly and its sign is inverted, a phenomenon already described by Meijer and coworkers.[47] Upon fast cooling, a metastable, chiral aggregate is formed. This is a kinetically favored process, while upon slow cooling, the thermodynamically most stable form is obtained. In general, the sign of the bisignate Cotton effect is correlated with the handedness of the helical stacking of the polymer chains. Slow cooling results in right-handed helically stacked aggregates while fast cooling results in a left-handed stacking. The magnitude of the CD signal is mainly governed by the distance and the angle between polymer chains.[48−50]

From these experiments, we can conclude that annealing has an important influence on the fraction of aggregates, as illustrated by the presence of the red-shifted, aggregation-related absorption band, and the shape of the aggregates, governing the intensity and the sign of the Cotton effects in the CD spectrum. It is important to note that the π-interactions themselves do not need to be different. They are essentially governed by the molecular structure, which is the same in all samples.

It must be mentioned that due to their different history, spin-coated films and powders obtained by precipitation can have a significant different history. However, here we compare a film which was molten (and therefore, its history was erased) and molten powders. In both cases, the history (cooling starting from melt) and the heat treatment (slow or fast cooling) were the same. Therefore, these samples can be compared, provided that any mass effect is ruled out. This means that the observed effects, visualized by UV−vis and CD spectroscopy, should be independent of the amount of material used. In this respect, films with

various thicknesses (**P3** spin-coated from chloroform solutions; 9.4, 24, and 40 mg/mL) were prepared and subjected to the same annealing procedures. Their UV−vis and CD spectra were recorded (see Figure S5). The g_{abs} value of HT-P3AT can be considered as an intrinsic material property and should therefore be independent of the film thickness.[51] This would imply that annealing has the same effect on all samples, no matter how much material is used. The g_{abs} value was calculated (Figure 5), showing no effect of the film thickness for the samples before annealing and those subjected to fast cooling. The slow-cooling procedure, however, shows a slight film thickness dependent behavior of the g_{abs} value—the thinnest films showing the strongest chiral effects. Both observations indicate small differences in the structural parameters of the supramolecular aggregates, depending on the film thickness. Similar results were reported by Joshi et al.,[52] using XRD to demonstrate the influence of the film thickness on the crystalline structure of HT-P3AT. In summary, before annealing and upon fast cooling, the g_{abs} value is thickness-independent, probably due to a rather low degree of organization. However, upon slow cooling, the g_{abs} value is higher and also shows some thickness dependence, probably caused by differences in the structural parameters of the supramolecular π-stacks. Fortunately, at $\lambda \sim 615$ nm, the wavelength of the red-shifted absorption band, the deviation is relatively small. Therefore, the relevant chiroptical properties, measured on spin-coated films, can be correlated with the magnetic properties measured for which the thicker, pressed films were used.

ESR Spectroscopy. The magnetic behavior of all polymer powder samples was initially studied by ESR spectroscopy at 300 K. The samples were treated with an alcoholic hydrazine solution and dried under argon to avoid polaron formation by oxidation to ambient air. The inferred spin densities, g values, and line widths are reported in Table 2.

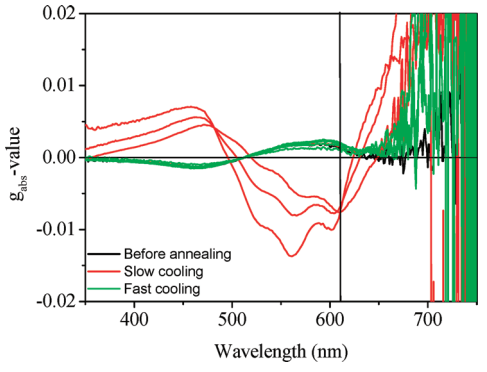

Figure 5. g_{abs} value for **P3** films of different thicknesses and subjected to different annealing procedures.

Upon variation of the molar mass (**P1**−**4**), clear changes are observed in the spectral line shape. The low molar mass polymers (**P1,2**) show a single line at zero crossing g value 2.0036 (spectra: see Figure S6). For higher molar masses (**P3,4**), two different, overlapping signals, S1 and S2, are present. The line shape of signal S2 is Lorentzian, while signal S1 could be adequately fitted by a Voigt shape of Lorentzian/Gaussian fraction of 2 and 0.5 for sample **P3** and **P3-slow**, respectively, allowing the determination of the g values and line widths of both signals (Table 2 and Figure 6). These observations indicated the presence of two types of spin centra which experience a different magnetic environment. In addition, noteworthy is that at higher molar masses the relative intensity of the S2 system increases compared to S1.

The influence of sample annealing on the spin properties was also monitored. **P3-fast** shows a similar ESR spectrum as **P3**. Two overlapping signals, corresponding to the presence of two different spin systems, are observed, and the relative intensity of both spectral lines is the same for both samples. On the other hand, **P3-slow** shows a significant increase in the relative intensity of S2, as shown in Figure 6. Clearly, annealing has an influence on the ratio of S1 and S2.

As the molecular structure of all samples is the same, the different spin systems S1 and S2 must originate from differences in the supramolecular structure.[53−55] A powder sample of HT-P3AT typically consists of well-ordered, aggregated polymer chains with unaggregated regions from the chain end groups. Both the aggregates and the amorphous regions contain unpaired electrons, which behave differently. In the highly ordered aggregates, the spins (S2) are strongly delocalized. This behavior is confirmed by the g value, which is close to the free electron g value. Indeed, the spins do not seem to interact with their environment as this would give rise to a shift of the g factor. Also, any signs of hyperfine interaction is absent, supporting the delocalized nature of S2. In addition, the line widths are significantly more narrow ascribed to the motional narrowing effect.[54] The first spin system (S1), on the other hand, is located in the more amorphous regions. The spins are less delocalized, and deviations from the free electron g value are observed, ascribed to spin−orbit coupling. In addition, the line widths increase as the contribution of the Elliott mechanism,[56,57] causing line broadening at elevated temperatures, overwhelms the motional narrowing effect.

Increasing the molar mass (**P1**−**4**) increases the relative intensity of S2 relative to S1. This means that the fraction of

Table 2. ESR Spin Densities ($S = 1/2$), g Value, and Line Widths (ΔB_{pp}) Observed on Different Samples P1−4 before and after Annealing[a]

	S1			S2		
polymer	spin density[b] (10^{16} spins/g)	g value (±0.0001)	ΔB_{pp} (±0.1 G)	spin density[b] (10^{16} spins/g)	g value (±0.0001)	ΔB_{pp} (G)
P1	1.3	2.0037	6.9			
P2	1.8	2.0036	5.3			
P3	0.94	2.0042	5.4	0.27	2.0023	2.7
P4	1.4	2.0043	5.2	1.1	2.0023	2.8
P3-fast	0.48	2.0045	5.3	0.18	2.0022	2.8
P3-slow	2.1	2.0041	5.3	1.1	2.0022	1.4

[a] S1 and S2 refer to the two different signals observed. All measurements were performed at 300 K. [b] Accuracy estimated at ≤10%

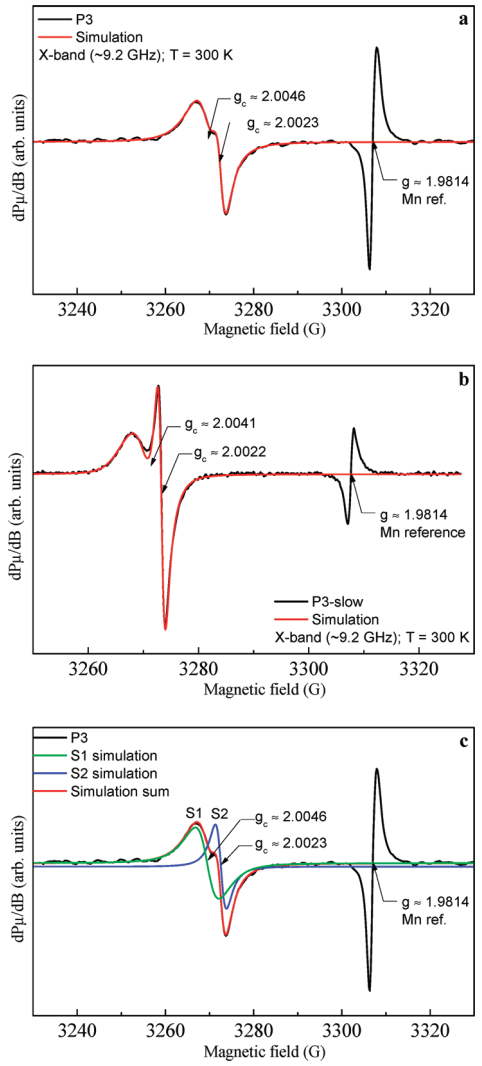

Figure 6. X-band first-derivative absorption ESR spectra of (a) **P3**, (b) **P3-slow**, and (c) simulation of the **P3** spectrum, using P_μ = 0.1 mW and B_m = 0.25 G. The narrow signal at the right stems from a comounted MgO:Mn^{2+} marker signal. The red solid curves represent the optimized simulation results using a Lorentzian shape for signal S2 and a Voigt function of Lorentz/Gauss fraction of 2 and 0.5 for the cases (a) and (b), respectively, leading to the data indicated in Table 2.

highly delocalized spins increases, which is consistent with a larger crystalline fraction upon increasing the molar mass. In this perspective, the behavior of **P3-slow** is also explained. Upon slow cooling of the polymer melt, the amount of well-organized aggregates increases, which is accompanied by an increasing intensity of the S2 system.

Finally, the temperature dependence of the magnetic susceptibility was studied for both spin systems. As presented in Figure 7, both spin systems show a paramagnetic Curie−Weiss behavior, which confirms the absence of interactions between the unpaired electrons.

SQUID Magnetometry. The magnetic behavior of **P1**−**4** was investigated by temperature-dependent SQUID magnetometry. From the magnetization (M) versus the applied magnetic field (H) curves, a diamagnetic contribution, caused by the large number of paired spins and sample holder, was subtracted. All samples show a weak ferromagnetic hysteretic behavior at 5 K

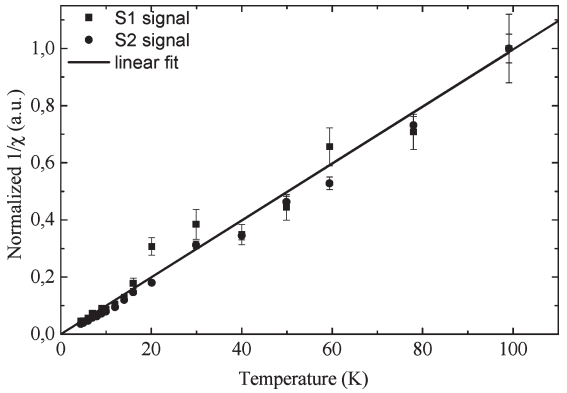

Figure 7. Temperature dependence of the magnetic susceptibility of **P3**, measured by ESR spectroscopy. Both spin systems S1 and S2 show a paramagnetic Curie−Weiss behavior.

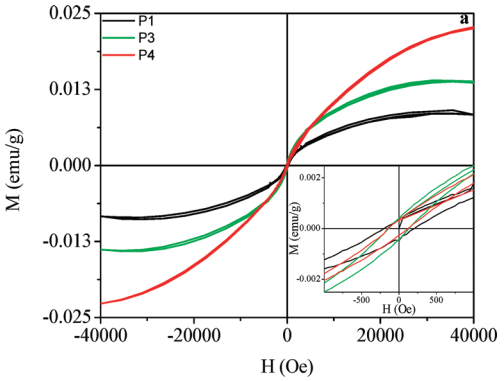

Figure 8. Magnetic hysteresis loops of **P1,3,4** at 5 K.

(for **P1,3,4**, see Figure 8), which is in accordance with the observations made earlier for **P2** (see Figure S7).[26] The magnitude of this ferromagnetism is characterized by the coercivity and is the same for all samples (~180 Oe). The magnetization at saturation, on the contrary, is clearly influenced by the molar mass of the samples. **P4**, which has the highest molar mass, shows the highest saturation magnetization, while **P1** the lowest. In addition, the $M(H)$ curves at 300 K showed a superparamagnetic behavior. Since the magnitude of the signal at 300 K equals the uncertainty of the background subtraction, no further conclusions could be drawn.

Similar results were obtained upon sample annealing, as depicted in Figure 9. The magnetic behavior was again evaluated at 5 and 300 K, showing a ferromagnetic and superparamagnetic behavior, respectively. At low temperature (Figure 9a), all samples show a similar coercive field (~180 Oe), but again clearly differ in the value of their saturation magnetization. The procedure in which **P3** was melted and slowly cooled (**P3-slow**) gives rise to the highest magnetization values, while **P3** before treatment and after fast cooling (**P3-fast**) show an almost identical saturation magnetization value. At room temperature (Figure 9b), a similar trend is observed; i.e., the highest saturation magnetization occurs for **P3-slow**.

The results suggest a relationship between the supramolecular organization of HT-P3AT and the magnetic behavior. Usually, magnetism is related to the presence of unpaired electrons. All HT-P3AT samples indeed contain low amounts of spins, even in

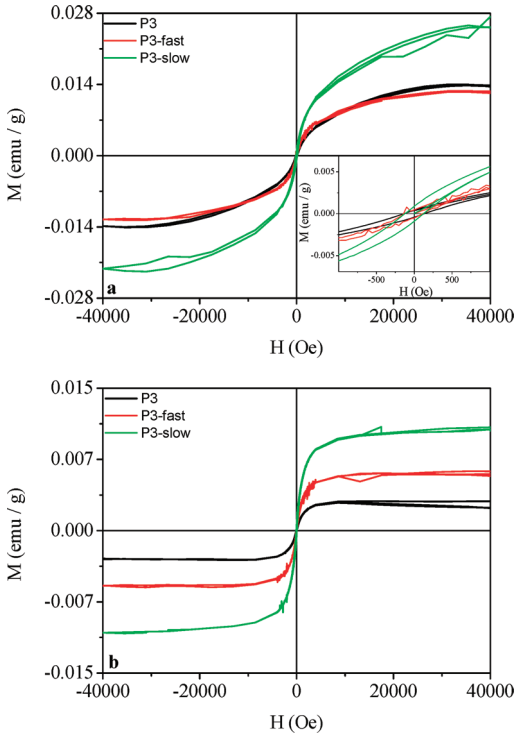

Figure 9. Magnetic hysteresis loops of **P3** subjected to different annealing conditions: (a) M/H behavior at 5 K; (b) M/H behavior at 300 K.

Table 3. Comparison of the ESR-Derived Spin Density and the Number of Bohr Magnetons, Determined by SQUID Magnetometry

polymer	spin density (10^{16} spins/g)[a]	Bohr magnetons (10^{17}/g)[b]	ratio[c]
P1	1.3	3.1	0.041
P3	1.2	3.1	0.039
P4	2.5	1.7	0.155
P3-fast	0.66	6.5	0.010
P3-slow	3.2	12	0.025

[a] Sum of S1 and S2 signals, determined by ESR at 300 K. [b] Determined by SQUID at 300 K. [c] Ratio of the spin density and the number of Bohr magnetons.

the neutral state, as was revealed by ESR spectroscopy. However, the number of ESR-active centra does not correspond to the number of Bohr magnetons, derived from the saturation magnetization (SQUID).[26] As evident from Table 3, the number of Bohr magnetons significantly exceeds the ESR values, suggesting the presence of an additional spin system, apparently not resolved by ESR spectroscopy. On the other hand, this spin system gives rise to a small but clearly observable magnetic hysteresis effect at 5 K. These results suggest that this contribution originates from another mechanism, such as orbital magnetism, possibly associated with the aromatic repeating units of the conjugated polymer backbone.[58,59] It must be mentioned that chirality or the helicity of the stacked polymer chains is not required for this contribution, as similar results are obtained in achiral P3ATs, in which the polymer chains stack in a parallel fashion.[26]

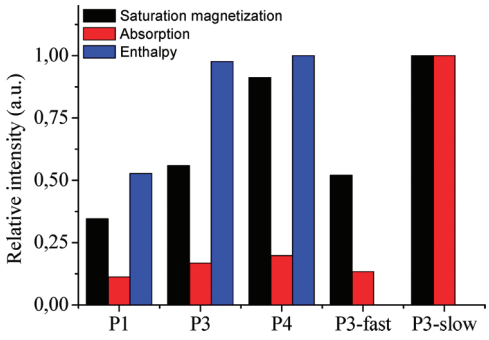

Figure 10. Comparison of the relative intensity of the saturation magnetization determined from SQUID measurements at 5 K, the red-shifted absorption band and the enthalpy of fusion, determined by DSC.

In contrast, a clear correlation is observed between the number of Bohr magnetons and the strength of the red-shifted absorption band which originates from multiple, strongly interacting polymer chains. Both the molar mass and annealing have a significant influence on the saturation magnetization. As evidenced in Figure 10, an increase in the amount of strongly interacting, planar polymer chains, quantified by taking the relative integration of the red-shifted absorption band, induces higher magnetization values at saturation. However, a similar number of Bohr magnetons are found in poly(3-alkoxythiophene)s (P3AOT),[26,37,60] which do not organize into large aggregates. The typical, red-shifted absorption band is in these materials also absent. As a consequence, the high number of Bohr magnetons in the case of HT-P3AT cannot exclusively be ascribed to aggregation nor to π-interactions. The observed trend between the saturation magnetization and the aggregation-related absorption band must therefore be a manifestation of some underlying effect. As P3ATs aggregate, the polymer chains are planarized, allowing the π-systems of different chains to interact. Upon increasing the amount of aggregates in a sample, for instance by changing the molar mass or by annealing, a higher fraction of such planar polymer chains is present. This suggests a possible relationship between the fraction of planar polymer chains, found by UV−vis spectroscopy and/or DSC and the saturation magnetization (Figure 10). In this perspective, our hypothesis explains the high number of Bohr magnetons observed for HT-P3AOT in which S−O interactions[61] induce a planar polymer conformation, which is for example also reflected in its large λ_{max} value. In summary, the high number of Bohr magnetons is related to the planarization of the polymer backbone.

The effects of the supramolecular behavior on the coercivity were also monitored. However, the coercive field is clearly independent of the degree of ordering. In addition, changing the shape of the aggregates by varying the annealing procedure, as nicely illustrated by CD spectroscopy, does not have a distinct effect on the coercive field. Clearly, changes on a supramolecular level are not able to induce deviations of the coercivity. On the other hand, as shown in our previous work, changing the nature of the substituent does result in a variation of the coercivity. For instance, head-to-tail poly(3-alkylthiothiophene)s (HT-P3ATTs) have a remarkably higher coercive field compared to HT-P3AT. Clearly, the coercivity is influenced by the molecular structure of the polymer and, closely related to this parameter, by the efficiency in which π-systems overlap. As all the samples under discussion in this article concern HT-P3ATs with the same

substituent, which all show a similar π-interaction, the coercivities can indeed be understood to be the same.

CONCLUSION

In conclusion, samples of HT-P3AT with different molar masses (**P1**−**4**) were prepared by fractionation. The chiroptical behavior was evaluated, showing a correlation between the relative intensity of the red-shifted, aggregation-related absorption band and the molar mass. In addition, in the CD spectrum, a monosignate Cotton effect is revealed with this distinct absorption, which can be ascribed to a transition that is delocalized over multiple stacked polymer chains. Also, the influence of thermal annealing on the chiroptical behavior of **P3** was evaluated. A different cooling rate clearly has a significant effect on the number and shape of the aggregates, as illustrated by UV−vis and CD spectroscopy.

Powder samples of **P1**−**4** and annealed powder samples (**P3-fast**/**slow**) were characterized by ESR spectroscopy and SQUID magnetometry. The ESR spectra of the high molar mass polymers **P3,4** consist of two lines: one of Lorentzian shape and the other of Voigt shape. The spectral characteristics (g value and line width) indicate the presence of two spin systems, i.e., highly delocalized spins situated in the crystalline domains, giving rise to a sharp signal and more confined spins localized in the amorphous part, corresponding to a broader line shape. The intensity of the signal is influenced by the molar mass and by annealing, as this affects the crystallinity. However, as previously reported, these spin systems are paramagnetic. SQUID magnetometry shows for all samples a ferromagnetic behavior at 5 K and a superparamagnetic behavior at 300 K. Upon increasing the molar mass and upon slow annealing, the saturation magnetization increases. Remarkably, the coercivity remains constant for all samples. We hypothesize that the magnitude of the magnetization is governed by the fraction of planar polymer chains, while the coercivity seems to depend on the molecular structure and, related to this, the efficiency of π-interactions between different polymer chains.

ASSOCIATED CONTENT

Supporting Information. GPC traces and ^{1}H NMR spectra of the different polymer fractions, the UV−vis spectra of **P1**−**4** in chloroform, and the deconvolution of the UV−vis spectra of **P1**−**4** upon aggregation and annealing; UV−vis and CD spectra concerning the influence of the film thickness (of **P3**, upon annealing) on the supramolecular behavior; ESR spectra of **P1,2,4** and **P3-fast**; $M(H)$ behavior of **P2** (5 and 300 K) and **P1**−**4** (at 300 K). This material is available free of charge via the Internet at http://pubs.acs.org.

AUTHOR INFORMATION

Corresponding Author

*E-mail: guy.koeckelberghs@chem.kuleuven.be.

ACKNOWLEDGMENT

We are grateful to the Fund for Scientific Research (FWO-Vlaanderen), the Flemish Concerted Action (GOA), the Belgian Interuniversity Poles of Attraction (IAP), and the Air Force Office of Scientific Research. J.C. is a doctoral fellow of the Institute for the Promotion of Innovation through Science and Technology in Flanders (IWT-Vlaanderen).

REFERENCES

(1) *Handbook of Conducting Polymer*, 3rd ed.; Skotheim, T. A., Reynolds, J. R., Eds.; CRC Press: Boca Raton, FL, 2007.
(2) Brédas, J. L.; Street, G. B. *Acc. Chem. Res.* **1985**, *18*, 309.
(3) Fisher, A. J.; Hayes, W.; Wallace, D. S. *J. Phys.: Condens. Matter* **1989**, *1*, 5567.
(4) Ikoma, T.; Okada, S.; Nakanishi, H.; Akiyama, K.; Tero-Kubota, S.; Mobius, K.; Weber, S. *Phys. Rev. B* **2002**, *66*, xxxx.
(5) Sercheli, M. S.; Walmsley, L.; Rettori, C.; Correa, A. A.; Bulhoes, L. O. S.; Pereira, E. C. *Phys. Status Solidi B* **2000**, *220*, 631.
(6) Ovchinnikov, A. A. *Theor. Chim. Acta* **1978**, *47*, 297.
(7) Borden, W. T.; Davidson, E. R. *J. Am. Chem. Soc.* **1977**, *99*, 4587.
(8) Kothe, G.; Denkel, K. H.; Summerma., W. *Angew. Chem., Int. Ed.* **1970**, *9*, 906.
(9) Rajca, A.; Rajca, S. *J. Chem. Soc., Perkin Trans. 2* **1998**, 1077.
(10) Tomioka, H.; Hattori, M.; Hirai, K.; Sato, K.; Shiomi, D.; Takui, T.; Itoh, K. *J. Am. Chem. Soc.* **1998**, *120*, 1106.
(11) Rajca, A.; Rajca, S.; Wongsriratanakul, J. *J. Am. Chem. Soc.* **1999**, *121*, 6308.
(12) Nishide, H.; Maeda, T.; Oyaizu, K.; Tsuchida, E. *J. Org. Chem.* **1999**, *64*, 7129.
(13) Kaneko, T.; Makino, T.; Miyaji, H.; Teraguchi, M.; Aoki, T.; Miyasaka, M.; Nishide, H. *J. Am. Chem. Soc.* **2003**, *125*, 3554.
(14) Murata, H.; Miyajima, D.; Nishide, H. *Macromolecules* **2006**, *39*, 6331.
(15) Long, Y.; Chen, Z.; Shen, J.; Zhang, Z.; Zhang, L.; Xiao, H.; Wan, M.; Duvail, J. L. *J. Phys. Chem. B* **2006**, *110*, 23228.
(16) Zaidi, N. A.; Giblin, S. R.; Terry, I.; Monkman, A. P. *Polymer* **2004**, *45*, 5683.
(17) Dallas, P.; Stamopoulos, D.; Boukos, N.; Tzitzios, V.; Niarchos, D.; Petridis, D. *Polymer* **2007**, *48*, 3162.
(18) Kahol, P. K.; Raghunathan, A.; McCormick, B. J. *Synth. Met.* **2004**, *140*, 261.
(19) Mizoguchi, K.; Kachi, N.; Sakamoto, H.; Kume, K.; Yoshioka, K.; Masubuchi, S.; Kazama, S. *Synth. Met.* **1997**, *84*, 695.
(20) Nascimento, O. R.; de Oliveira, A. J. A.; Pereira, E. C.; Correa, A. A.; Walmsley, L. *J. Phys.: Condens. Matter* **2008**, 035214 (8 pp).
(21) de Paula, F. R.; Walmsley, L.; Pereira, E. C.; de Oliveira, A. J. A. *J. Magn. Magn. Mater.* **2008**, *320*, E193.
(22) Sugiyama, K.; Kojima, T.; Fukuda, H.; Yashiro, H.; Matsuura, T.; Shimoyama, Y. *Thin Solid Films* **2008**, *516*, 2691.
(23) Nalwa, H. S. *Phys. Rev. B: Condens. Matter* **1989**, *39*, 5964.
(24) Konkin, A.; Roth, H. K.; Scharff, P.; Aganov, A.; Ambacher, O.; Sensfuss, S. *Solid State Commun.* **2009**, *149*, 893.
(25) Nechtschein, M.; Devreux, F.; Genoud, F.; Guglielmi, M.; Holczer, K. *Phys. Rev. B: Condens. Matter* **1983**, *27*, 61.
(26) Vandeleene, S.; Jivanescu, M.; Stesmans, A.; Cuppens, J.; Van Bael, M. J.; Yamada, H.; Sato, N.; Verbiest, T.; Koeckelberghs, G. *Macromolecules* **2010**, *43*, 2910.
(27) Chabinyc, M. L. *Polym. Rev.* **2008**, *48*, 463.
(28) Stesmans, A. *Phys. Rev. B: Condens. Matter* **1993**, *48*, 2418.
(29) Loewe, R. S.; Ewbank, P. C.; Liu, J.; Zhai, L.; McCullough, R. D. *Macromolecules* **2001**, *34*, 4324.
(30) Ishikawa, H.; Xu, X. F.; Kobayashi, A.; Satoh, M.; Suzuki, M.; Hasegawa, E. *J. Phys. D: Appl. Phys.* **1992**, *25*, 897.
(31) Ishikawa, H.; Amano, K.; Kobayashi, A.; Satoh, M.; Hasegawa, E. *Synth. Met.* **1994**, *64*, 49.
(32) Hourquebie, P.; Olmedo, L. *Synth. Met.* **1994**, *65*, 19.
(33) Trznadel, M.; Pron, A.; Zagorska, M. *Macromolecules* **1998**, *31*, 5051.
(34) Zahn, S.; Swager, T. M. *Angew. Chem., Int. Ed.* **2002**, *41*, 4225.
(35) Babudri, F.; Colangiuli, D.; Di Bari, L.; Farinola, G. M.; Omar, O. H.; Naso, F.; Pescitelli, G. *Macromolecules* **2006**, *39*, 5206.
(36) Brown, P. J.; Thomas, D. S.; Kohler, A.; Wilson, J. S.; Kim, J. S.; Ramsdale, C. M.; Sirringhaus, H.; Friend, R. H. *Phys. Rev. B* **2003**, *67*.
(37) Vangheluwe, M.; Verbiest, T.; Koeckelberghs, G. *Macromolecules* **2008**, *41*, 1041.

(38) Vandeleene, S.; Van den Bergh, K.; Verbiest, T.; Koeckelberghs, G. *Macromolecules* **2008**, *41*, 5123.
(39) Bilo, E. J. *Excel for Chemists*, 2nd ed., 2001.
(40) Zen, A.; Saphiannikova, M.; Neher, D.; Grenzer, J.; Grigorian, S.; Pietsch, U.; Asawapirom, U.; Janietz, S.; Scherf, U.; Lieberwirth, I.; Wegner, G. *Macromolecules* **2006**, *39*, 2162.
(41) Liu, J. H.; Arif, M.; Zou, J. H.; Khondaker, S. I.; Zhai, L. *Macromolecules* **2009**, *42*, 9390.
(42) Wu, Z. Y.; Petzold, A.; Henze, T.; Thurn-Albrecht, T.; Lohwasser, R. H.; Sommer, M.; Thelakkat, M. *Macromolecules* **2010**, *43*, 4646.
(43) Pascui, O. F.; Lohwasser, R.; Sommer, M.; Thelakkat, M.; Thurn-Albrecht, T.; Saalwachter, K. *Macromolecules* **2010**, *43*, 9401.
(44) Virkar, A. A.; Mannsfeld, S.; Bao, Z. A.; Stingelin, N. *Adv. Mater.* **2010**, *22*, 3857.
(45) Brinkmann, M.; Rannou, P. *Macromolecules* **2009**, *42*, 1125.
(46) Muller, C.; Zhigadlo, N. D.; Kumar, A.; Baklar, M. A.; Karpinski, J.; Smith, P.; Kreouzis, T.; Stingelin, N. *Macromolecules* **2011**, *44*, 1221.
(47) Bouman, M. M.; Meijer, E. W. *Adv. Mater.* **1995**, *7*, 385.
(48) Rodger, A.; Nordén, B. *Circ. Dichroism Linear Dichroism* **1997**.
(49) Cornelis, D.; Peeters, H.; Zrig, S.; Andrioletti, B.; Rose, E.; Verbiest, T.; Koeckelberghs, G. *Chem. Mater.* **2008**, *20*, 2133.
(50) Purdie, N.; Brittain, H. G. *Anal. Appl. Circ. Dichroism* **1994**.
(51) Lakhwani, G.; Koeckelberghs, G.; Meskers, S. C. J.; Janssen, R. A. J. *Chem. Phys. Lett.* **2007**, *437*, 193.
(52) Joshi, S.; Grigorian, S.; Pietsch, U. *Phys. Status Solidi A* **2008**, *205*, 488.
(53) Sitaram, V.; Sharma, A.; Bhat, S. V.; Mizoguchi, K.; Menon, R. *Phys. Rev. B* **2005**, 72.
(54) Kanemoto, K.; Kato, T.; Aso, Y.; Otsubo, T. *Phys. Rev. B* **2003**, 68.
(55) Kanemoto, K.; Furukawa, K.; Negishi, N.; Aso, Y.; Otsubo, T. *Phys. Rev. B* **2007**, 76.
(56) Elliott, R. J. *Phys. Rev.* **1954**, *96*, 266.
(57) Mizoguchi, K.; Honda, M.; Kachi, N.; Shimizu, F.; Sakamoto, H.; Kume, K. *Solid State Commun.* **1995**, *96*, 333.
(58) Himmerich, M.; van Dongen, P. G. J.; Noack, R. M. *Eur. Phys. J. B* **2006**, *51*, 5.
(59) O'Hare, A.; Kusmartsev, F. V.; Kugel, K. I.; Laad, M. S. *Phys. Rev. B* **2007**, 76.
(60) Koeckelberghs, G.; Vangheluwe, M.; Samyn, C.; Persoons, A.; Verbiest, T. *Macromolecules* **2005**, *38*, 5554.
(61) Villa, E.; Agosti, E.; Castiglioni, C.; Gallazzi, M. C.; Zerbi, G. *J. Chem. Phys.* **1996**, *105*, 9461.